ANALYSIS OF A GEOMETRICAL MULTISCALE MODEL BASED ON THE COUPLING OF ODE'S AND PDE'S FOR BLOOD FLOW SIMULATIONS

ALFIO QUARTERONI[†] [‡] [§] AND ALESSANDRO VENEZIANI[‡] [§]

Abstract. In hemodynamics, local phenomena, such as the perturbation of flow pattern in a specific vascular region, are strictly related to the global features of the whole circulation (see e.g. [7]). In [16] we have proposed a heterogeneous model where a local, accurate, 3D description of blood flow by means of the Navier-Stokes equations in a specific artery is coupled with a systemic, 0D, lumped model of the remainder of circulation. This is a geometrical multiscale strategy, which couples an initial-boundary value problem to be used in a specific vascular region with an initial-value-problem in the rest of the circulatory system. It has been succesfully adopted to predict the outcome of a surgical operation (see [2, 3]). However, its interest goes beyond the context of blood flow simulations, as we point out in the Introduction. In this paper we provide a well posedness analysis of this multiscale model, by proving a local-in-time existence result based on a fixed-point technique. Moreover, we investigate the role of matching conditions between the two submodels for the numerical simulation.

Key words. Geometrical multiscale models, Blood flow simulations, Fixed-point techniques.

AMS subject classifications. 35M20,35Q30,76D03,65L05,76Z05

1. Introduction.

In computational fluid dynamics there might be the need of accurately simulating the flow in a subregion of a complex system, that can be reasonably represented by a hydraulic network. One may think, for instance, to a system for water supply for which there is the interest of ascertaining the spatial variations of velocity and pressure only in a specific pipeline or in a reservoir. Another instance, which has motivated our investigation, is the blood circulatory system. Here the underlying (low cost) model is based on an analogy with electric circuits and can predict the time evolution of average physical quantities (flow rate and pressure) in the different compartments of the overall system (see e.g. [15], [23]). Yet, there is the interest of carrying out three-dimensional simulations on a sensible region (e.g. a coronary by-pass, a carotid bifurcation, a stented artery, etc.). In these cases, the local investigation requires the specification of boundary conditions on the interface between the region of interest and the remainder of the network. In fact, the significance of numerical results is strictly related to the capability of the numerical device of properly accounting for exchange of information with the global network. Actually, it is well known that, in the circulatory system, local behavior of blood flow in a specific region is strictly related to the systemic features of the circulation. For instance, the presence of a plaque localized in a carotid bifurcation can induce a flow rate increment in other vessels in order to restore a sufficient oxygenation of the brain, thus modifying the local flow features (see [1]).

Blood is a complex fluid, which can be described by means of the incompressible Navier-Stokes equations (possibly accounting for a non Newtonian rheology - see

[†]IMA and Inst. Bernoulli, École Polytechnique Fédérale de Lausanne, CH-1024 Switzerland alfio.quarteroni@epfl.ch

[‡]MOX (Modeling and Scientific Computing), Dipartimento di Matematica "F. Brioschi",Politecnico di Milano,Via Bonardi 9, I - 20133 Milano, Italy,

[§]This work has been supported by Cofin2000 MURST Project, by the Special Project "Large Scale Computing: Multiscale Computing in Biofluiddynamics" of the Politecnico di Milano and the Swiss National Science Foundation Project n. 21-54139.98.

[17]). Numerical simulations of the whole circulatory system completely based on the numerical solution of the Navier-Stokes equations are unaffordable. Actually, a tremendous amount of morphological data would be required, which typically are not available, not to mention the computational costs of such investigations which would be prohibitive. In order to set up numerical tools for the correct simulation of blood flow, in [7] we have proposed a *geometrical multiscale* approach. In fact, a hierarchy of models was introduced, with a different level of accuracy, ranging from the local 3D accurate Navier-Stokes equations to systems of ordinary differential equations: the latter are associated to lumped parameter models set up by exploiting the analogy between hydraulic and electric networks (see e.g. [23]) and account for the systemic circulation. These different models are then coupled at the numerical level in order to provide at the same time local details and global information on blood flow. The same strategy has been succesfully used in [5] for the coupling of a 3D model with a 1D model based on a non-linear hyperbolic system that accounts for the propagation of pressure waves in the arterial tree.

A heterogeneous model which couples ordinary differential systems for the whole circulation with the 3D Navier-Stokes equations has been proposed in [16] and succesfully adopted in a real-life application arising from pediatric surgery (see [2, 3]).

The aim of the present work is to provide a theoretical analysis of this heterogeneous model coupling ODE's and PDE's, providing a local-in-time existence result for the solution. The heterogeneous problem will actually be split into subproblems (the system of ODE's for the global description and the PDE system based on the Navier-Stokes equations for the local model). The solution of the original problem will be regarded as the solution of a suitable fixed point problem, based on the successive solution of the subproblems. A-priori estimates for the solutions of the individual subproblems will be stated at first. Then, we will prove that the classical Schauder fixed point theorem can be applied in order to prove the existence of the solution of the original problem.

The outline of this paper is as follows. In §2 we address the analysis of the Navier-Stokes problem, having provided boundary conditions which can be considered as a generalization of the so-called mean pressure drop problem investigated in [10], as they arise in bioengineering applications. The well-posedness analysis carried out for the mean pressure drop problem is therefore generalized to the present case. In §3 we discuss the basic features of the ordinary differential systems arising in the systemic modelling. We will address the lumped parameter description of a simple compliant pipe and then extend the basic concepts to the case of a nonlinear ODE system accounting for the whole circulation. In §4 we deal with the heterogeneous model obtained by coupling the local and the systemic submodels. In §5 we address the well-posedness analysis and prove our main result. We comment on the way the interface conditions can be split to set up an iterative algorithm for the numerical solution of the coupled multiscale problem. Finally, in §6 we provide some numerical results on academic test cases as well as on a case of real life clinical interest.

1.1. Basic Notations. Let Ω be a bounded domain in $\mathbb{R}^d$ $(d = 2, 3)$. We denote by $L^2(\Omega)$ the space of real functions whose square is integrable in Ω and by $(\cdot,\cdot)$ and $\|\cdot\|$ the associated inner product and norm, respectively. The corresponding vector space $(L^2(\Omega))^d$ will be denoted by $\mathbf{L}^2(\Omega)$. Similarly, we introduce the space $H^1(\Omega) = \{v \in L^2(\Omega) | \nabla v \in \mathbf{L}^2(\Omega)\}$ whose norm is denoted $\|\cdot\|_1$. Correspondingly, we set $\mathbf{H}^1(\Omega) = (H^1(\Omega))^d$ and we still denote its norm by $\|\cdot\|_1$. For functions depending on space and time, for a given space $\mathbf{V}$ of space dependent functions, we define (for

some $T > 0$)

$$L^2(0,T;\mathbf{V}) = \{\mathbf{v} : (0,T) \to \mathbf{V} \,|\, \mathbf{v} \text{ is measurable and } \int_0^T \|\mathbf{v}(t)\|_{\mathbf{V}}^2 dt < \infty\}$$

with norm $\|\mathbf{v}\|_{L^2(0,T;\mathbf{V})} = \left(\int_0^T \|\mathbf{v}(t)\|_{\mathbf{V}}^2 dt\right)^{1/2}$ and

$$L^\infty(0,T;\mathbf{V}) = \{\mathbf{v} : (0,T) \to \mathbf{V} \,|\, \sup_{t\in(0,T)} \|\mathbf{v}(t)\|_{\mathbf{V}} < \infty\}$$

with norm $\|\mathbf{v}\|_{L^\infty(0,T;\mathbf{V})} = \sup_{t\in(0,T)} \|\mathbf{v}(t)\|_{\mathbf{V}}$.

If Σ is an open non-empty subset of $\partial\Omega$, we denote by $H^{1/2}(\Sigma)$ the space of functions defined on Σ which are traces of functions in $H^1(\Omega)$. We recall that the trace operator $\mathcal{L}_{\text{trace}} : H^1(\Omega) \to H^{1/2}(\partial\Omega)$ is surjective and continuous (see [12]).

When considering functions which depend only on time, we define the space:

$$\mathbf{L}^\infty(0,T) = \{\mathbf{z} : (0,T) \to \mathbb{R}^m \,|\, \sup_{t\in(0,T)} |\mathbf{z}(t)| < \infty\}$$

endowed with the norm $\|\mathbf{z}\|_{\mathbf{L}^\infty(0,T)} = \sup_{t\in(0,T)} |\mathbf{z}(t)|$.

2. The local submodel. Let $\Omega \subset \mathbb{R}^3$ (or $\mathbb{R}^2$) be a vascular region where we aim at providing a detailed flow analysis. For each $\boldsymbol{\xi} \in \Omega$, and at any time $t > 0$, we denote by $\mathbf{u}(\boldsymbol{\xi}, t)$ and $p(\boldsymbol{\xi}, t)$ the blood velocity and pressure, respectively. Moreover, we assume that blood is an incompressible Newtonian fluid, which is acceptable in many situations, especially in large and medium-size vessels (see [17]). Correspondingly, we denote by ρ the blood density and by ν the blood viscosity, which are both assumed to be constant.

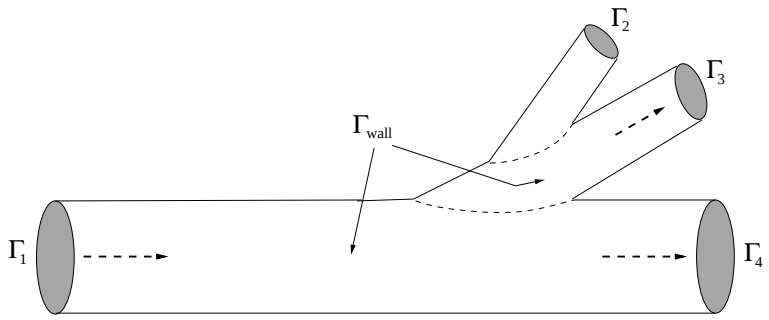

FIG. 2.1. *A typical vascular region, where the boundary* Γ_1 *represents the upstream section, while* Γ_i $(i = 2, 3, 4)$ *are the downstream sections.*

Under the previous assumptions, blood flow can be described by the Navier-Stokes equations

$$\begin{cases} \rho\dfrac{\partial \mathbf{u}}{\partial t} - \nu\Delta\mathbf{u} + \rho(\mathbf{u}\cdot\nabla)\mathbf{u} + \nabla p = \mathbf{0} \\ \nabla\cdot\mathbf{u} = 0 \end{cases} \qquad \boldsymbol{\xi} \in \Omega, t > 0, \tag{2.1}$$

which express momentum and mass conservation principles. We are neglecting the presence of any external force, which is reasonable in our context. For the sake of simplicity, we normalize ρ to 1. The previous system has to be provided with initial condition,

$$\mathbf{u}(\boldsymbol{\xi}, 0) = \mathbf{u_0}(\boldsymbol{\xi}) \qquad \boldsymbol{\xi} \in \Omega, \tag{2.2}$$

and boundary conditions. In this respect, we split $\partial\Omega$ into different parts. The vascular wall will be denoted by Γ_{wall}. In the present work, we are assuming that the walls are rigid, so that no-slip boundary condition

$$\mathbf{u}(\boldsymbol{\xi}, t) = 0 \qquad \boldsymbol{\xi} \in \Gamma_{wall}, t > 0 \tag{2.3}$$

hold. The other parts of $\partial\Omega$ are the artificial boundaries which bound the computational domain. For the sake of clarity, we distinguish the "upstream" or proximal sections, on the side of the heart, and the "downstream" or distal sections, on the side of the peripheral vessels. We will suppose in general that there are $\overline{n}$ artificial sections, denoted by Γ_i $(i = 1, \ldots, \overline{n})$, where we can prescribe different kind of boundary conditions, corresponding to different specific boundary problems (see e.g. [10, 5, 6, 22]). In the present work, we prescribe, in particular, the condition

$$p\mathbf{n} - \nu\nabla\mathbf{u}\cdot\mathbf{n} - R_i(\mathbf{u}\cdot\mathbf{n})\mathbf{n} = p_i\mathbf{n} \qquad \text{on } \Gamma_i, \tag{2.4}$$

where $p_i = p_i(t)$ is assumed to be a given function of t (independent of $\mathbf{x}$) on each section, $\mathbf{n}$ represents the outward unit vector on every part of the vessel boundary and R_i is a suitable non negative constant. When $R_i = 0$ we recover from (2.4) the conditions for the Navier-Stokes problem corresponding to the *mean pressure drop problem* investigated in [10], and specifically investigated in the context of hemodynamics in [22]. The physical justification for the case in which $R_i \neq 0$ is provided in the sequel (see Fig. 4.1).

Both the mathematical analysis and the numerical treatment of the Navier-Stokes problem are based on its weak formulation. We define the following bilinear and trilinear forms:

$$\begin{aligned} &a : \mathbf{H}^1(\Omega)\times\mathbf{H}^1(\Omega) \to \mathbb{R} \ \text{ s.t.} \\ &\quad a(\mathbf{v},\boldsymbol{\varphi}) = \nu(\nabla\mathbf{v},\nabla\boldsymbol{\varphi}) + \textstyle\sum_{i=1}^{\overline{n}} R_i \int_{\Gamma_i} (\mathbf{v}\cdot\mathbf{n})\mathbf{n}\cdot\boldsymbol{\varphi} d\boldsymbol{\gamma}, \end{aligned} \tag{2.5a}$$

$$b : \mathbf{H}^1(\Omega)\times\mathbf{H}^1(\Omega)\times\mathbf{H}^1(\Omega) \to \mathbb{R} \quad \text{s.t.} \quad b(\mathbf{v},\mathbf{w},\boldsymbol{\varphi}) = ((\mathbf{v}\cdot\nabla)\mathbf{w},\boldsymbol{\varphi}), \tag{2.5b}$$

$$l : Q\times\mathbf{H}^1(\Omega) \to \mathbb{R} \quad \text{s.t.} \quad l(\psi,\boldsymbol{\varphi}) = -(\psi,\nabla\cdot\boldsymbol{\varphi}), \tag{2.5c}$$

where $Q = L^2(\Omega)$. Moreover, we set

$$c(t,\boldsymbol{\varphi}) = -\sum_{i=1}^{\overline{n}} p_i(t) \int_{\Gamma_i} \mathbf{n}\cdot\boldsymbol{\varphi} d\boldsymbol{\gamma} \tag{2.5d}$$

for each $\boldsymbol{\varphi} \in \mathbf{H}^1(\Omega)$. Furthermore, we define:

$$\mathbf{V} = \{\boldsymbol{\varphi} \in \mathbf{H}^1(\Omega) \mid \boldsymbol{\varphi}|_{\Gamma_{wall}} = \mathbf{0}\}, \qquad \mathbf{V}^* = \{\boldsymbol{\varphi} \in \mathbf{V} \mid \nabla\cdot\boldsymbol{\varphi} = 0\}. \tag{2.6}$$

The weak formulation of the problem given by (2.1), (2.2), (2.3), (2.4) reads:

PROBLEM 2.1. *Given* $\mathbf{u_0} \in \mathbf{V}^*$ *and* $p_i \in L^\infty(0,T)$ *for* $i = 1, \ldots, \overline{n}$, *find* $\mathbf{u} \in L^2(0,T;\mathbf{V})$ *and* $p \in L^2(0,T,Q)$ *such that for all* $t > 0$

$$\begin{cases} \left(\dfrac{\partial \mathbf{u}}{\partial t}, \boldsymbol{\varphi}\right) + a(\mathbf{u}, \boldsymbol{\varphi}) + b(\mathbf{u}, \mathbf{u}, \boldsymbol{\varphi}) + l(p, \boldsymbol{\varphi}) = c(t, \boldsymbol{\varphi}) \qquad \forall \boldsymbol{\varphi} \in \mathbf{V} \\ \\ l(\psi, \mathbf{u}) = 0 \qquad \forall \psi \in Q \end{cases}$$

with $\mathbf{u}|_{t=0} = \mathbf{u_0}$. Its solenoidal version, which is more suitable for our analysis (see [10, 21]) reads:

PROBLEM 2.2. *Given* $\mathbf{u_0} \in \mathbf{V}^*$, *find* $\mathbf{u} \in L^2(0,T;\mathbf{V}^*)$ *such that for all* $t \geq 0$

$$\left(\frac{\partial \mathbf{u}}{\partial t}, \boldsymbol{\varphi}\right) + a(\mathbf{u}, \boldsymbol{\varphi}) + b(\mathbf{u}, \mathbf{u}, \boldsymbol{\varphi}) = c(\boldsymbol{\varphi}) \qquad \forall \boldsymbol{\varphi} \in \mathbf{V}^* \tag{2.7}$$

with $\mathbf{u}|_{t=0} = \mathbf{u_0}$.

2.1. Well-posedness analysis. Let $\mathbf{V}_1^*$ be the completion of $\mathbf{V}^*$ with respect to the norm of $\mathbf{L}^2(\Omega)$. For each $\mathbf{f} \in \mathbf{V}_1^*$ there exists exactly one $\mathbf{w} \in \mathbf{V}^*$ satisfying

$$(\nabla \mathbf{w}, \nabla \boldsymbol{\varphi}) = (\mathbf{f}, \boldsymbol{\varphi}) \qquad \forall \boldsymbol{\varphi} \in \mathbf{V}^*. \tag{2.8}$$

Conversely, for every $\mathbf{w} \in \mathbf{V}^*$ there exists at most one $\mathbf{f} \in \mathbf{V}_1^*$ such that (2.8) holds. In this way, as stated in [9], a one-to-one correspondence can be defined between the elements $\mathbf{f}$ of $\mathbf{V}_1^*$ and the functions $\mathbf{w}$ belonging to a suitable subspace $D(\tilde{\Delta})$ of $\mathbf{V}^*$. The Stokes operator $\tilde{\Delta} : D(\tilde{\Delta}) \to \mathbf{V}_1^*$ is defined setting $-\tilde{\Delta}\mathbf{w} = \mathbf{f}$ so that (2.8) is satisfied. The inverse operator $\tilde{\Delta}^{-1}$ is self-adjoint and has a sequence of eigenfunctions $\{\mathbf{a}_k\}$, which are orthogonal (see [21]) in $\mathbf{V}^*$.

In the sequel, c_i $(i = 1, 2, \ldots)$ will denote generic constants, not necessarily the same at different places. The inequalities

$$\sup_{\Omega} |\mathbf{w}| \leq c_1 \|\nabla \mathbf{w}\|^{1/2} \|\tilde{\Delta}\mathbf{w}\|^{1/2}, \tag{2.9}$$

$$\|\nabla \mathbf{w}\| \leq c_2 \|\tilde{\Delta}\mathbf{w}\| \tag{2.10}$$

are satisfied for each $\mathbf{w} \in D(\tilde{\Delta})$, provided Ω is a bounded domain (see [10, 25]). Furthermore, if we define

$$\tilde{p} = \sup_{t \geq 0} \sum_{i=1}^{\overline{n}} |p_i|, \quad R = \max_i R_i$$

the following estimates hold for every $\mathbf{w} \in \operatorname{span}\{\mathbf{a}_1, \ldots, \mathbf{a}_N\}$:

$$\left| \sum_{i=1}^{\overline{n}} p_i \int_{\Gamma_i} \tilde{\Delta}\mathbf{w} \cdot \mathbf{n} d\boldsymbol{\gamma} \right| \leq c_3 \tilde{p} \, \|\tilde{\Delta}\mathbf{w}\|, \tag{2.11}$$

$$\left| \sum_{i=1}^{\overline{n}} R_i \int_{\Gamma_i} (\mathbf{w} \cdot \mathbf{n}) \mathbf{n} \cdot \tilde{\Delta}\mathbf{w} d\boldsymbol{\gamma} \right| \leq c_4 R \|\nabla \mathbf{w}\| \, \|\tilde{\Delta}\mathbf{w}\|. \tag{2.12}$$

The former can be found in [10]. To prove (2.12) we start noting that for each $v \in H^1(\Omega)$ the identity

$$\int_{\partial\Omega} v\mathbf{n} \cdot \tilde{\Delta}\mathbf{w} = \sum_{i=0}^{i=\overline{n}} \int_{\Gamma_i} v\mathbf{n} \cdot \tilde{\Delta}\mathbf{w} = \int_{\Omega} v \nabla \cdot \tilde{\Delta}\mathbf{w} + \int_{\Omega} \nabla v \cdot \tilde{\Delta}\mathbf{w} = \int_{\Omega} \nabla v \cdot \tilde{\Delta}\mathbf{w} \tag{2.13}$$

holds since $\tilde{\Delta}\mathbf{w}$ is a solenoidal function vanishing on Γ_{wall}.

Indeed, let $v \in H^1(\Omega)$ satisfy:

$$\begin{aligned} &-\Delta v = 0 \quad \text{in } \Omega \\ &v|_{\Gamma_i} = R_i(\mathbf{w}\cdot\mathbf{n})|_{\Gamma_i}, \ i = 1,\dots,\overline{n} \\ &v|_{\Gamma_{wall}} = 0. \end{aligned}$$

From well known results on harmonic extensions we have (see [12]):

$$\|\nabla v\| \le \sum_{i=1}^{\overline{n}} R_i \|\mathbf{w}\cdot\mathbf{n}\|_{H^{1/2}(\Gamma)} \le c_4 R \|\nabla \mathbf{w}\|,$$

thus, (2.12) follows from (2.13).

Now, we can prove the following Proposition.

PROPOSITION 2.1. *Let ν and R be such that*

$$\kappa = \nu - 2Rc_2c_4 > 0. \tag{2.14}$$

Then, there is a time interval on which the solution of Problem 2.2 does exist. Furthermore, if we assume that the initial and boundary data are sufficiently small, precisely

$$\|\nabla \mathbf{u}_0\| < \frac{\kappa}{4c_1\sqrt{c_2}} \qquad \text{and} \qquad \tilde{p} < \frac{\sqrt{\nu\kappa^3}}{\sqrt{32c_2^3}c_1c_3}, \tag{2.15}$$

then, the solution of Problem 2.2 exists for all $t > 0$ and satisfies the inequality:

$$\|\nabla \mathbf{u}(t)\| \le \frac{\kappa}{4c_1\sqrt{c_2}}. \tag{2.16}$$

Finally, there exists an interval $(0,T)$ in which the solution is unique and depends continuously on the data.

Proof. This Proposition is an extension of a similar result holding for the mean pressure drop problem (Theorem 6 in [10]). Actually, as we have already pointed out, the mean pressure drop problem can be recovered as a particular case of Problem 2.2, when $R = 0$. We therefore report only the main steps of the proof.

Consider the sequence

$$\mathbf{u}_N = \sum_{k=1}^{N} \gamma_{kN}(t)\mathbf{a}_k$$

which is built by solving equation (2.7) for each $\boldsymbol{\varphi} \in \text{span}\{\mathbf{a}_1,\dots,\mathbf{a}_N\}$. The solution $\mathbf{u}$ is obtained as the weak limit of a subsequence of $\{\mathbf{u}_N\}$ in $L^2(0,T;\mathbf{V}^*)$. The outline of the proof is the following: we firstly obtain some a-priori estimates for $\{\mathbf{u}_N\}$ that are inherited by the limit solution when $N \to \infty$, yielding the existence of a solution locally in time. Then, if the initial data are small enough, we will prove further a-priori estimates, ensuring the existence of the solution for all $t > 0$. Finally, we will prove that locally in time the limit solution is unique and depends continuously on the data.

Setting $\boldsymbol{\varphi} = -\tilde{\Delta}\mathbf{u}_N$ in (2.7), we have

$$\frac{1}{2}\frac{d}{dt}\|\nabla \mathbf{u}_N\|^2 + \nu\|\tilde{\Delta}\mathbf{u}_N\|^2 = ((\mathbf{u}_N\cdot\nabla)\mathbf{u}_N, \tilde{\Delta}\mathbf{u}_N) + \sum_{i=1}^{\overline{n}} p_i \int_{\Gamma_i} \mathbf{n}\cdot\tilde{\Delta}\mathbf{u}_N$$

$$
\begin{aligned}
&+ \sum_{i=1}^{\overline{n}} R_i \int_{\Gamma_i} (\mathbf{u}_N \cdot \mathbf{n})\mathbf{n} \cdot \tilde{\Delta}\mathbf{u}_N, \\
&\leq \sup_{\Omega} |\mathbf{u}_N| \|\nabla \mathbf{u}_N\| \, \|\tilde{\Delta}\mathbf{u}_N\| + c_3 \tilde{p} \|\tilde{\Delta}\mathbf{u}_N\| \\
&+ c_4 R \|\nabla \mathbf{u}_N\| \, \|\tilde{\Delta}\mathbf{u}_N\| \\
&\leq c_1 \sqrt{c_2} \|\nabla \mathbf{u}_N\| \, \|\tilde{\Delta}\mathbf{u}_N\|^2 + \frac{c_3^2}{2\nu} \tilde{p}^2 + \frac{\nu}{2} \|\tilde{\Delta}\mathbf{u}_N\|^2 \\
&+ c_4 c_2 R \|\tilde{\Delta}\mathbf{u}_N\|^2.
\end{aligned}
$$

Therefore

$$
\frac{d}{dt}\|\nabla \mathbf{u}_N\|^2 + (\kappa - 2c_1\sqrt{c_2}\|\nabla \mathbf{u}_N\|) \, \|\tilde{\Delta}\mathbf{u}_N\|^2 \leq \frac{c_3^2}{\nu} \tilde{p}^2. \tag{2.17}
$$

Using standard arguments (see [10]), from this inequality we can infer that the Galerkin approximant $\mathbf{u}_N$ satisfies the following a-priori estimate:

$$
\|\mathbf{u}_N\|_{\mathbf{V}} \leq c\tilde{p} \tag{2.18}
$$

When $N \to \infty$, the same inequalitity is satisfied, locally in time, by the limit solution $\mathbf{u}$. This proves the local existence of a solution.

Furthermore, suppose that assumptions (2.14) and (2.15) hold. Then, there exists a time interval on which the coefficient of $\|\tilde{\Delta}\mathbf{u}_N\|^2$ is positive. Exploiting (2.10), we can prove that in the same interval:

$$
\|\nabla \mathbf{u}_N\| < \frac{\kappa}{4c_1\sqrt{c_2}}.
$$

The same inequality holds for the limit solution obtained for $N \to \infty$. It is then possible to prove that the sup of the time interval on which (2.16) holds, i.e. the time instant at which (2.16) becomes an equality, is not finite, yielding the global existence result.

Consider now the issue of uniqueness and continuous dependence on the data. We firstly prove that there exists a time interval of continuous dependence on the data, assuming the uniqueness of the solution. Later on, we will prove that the uniqueness actually holds. Suppose, therefore, that there exists a time interval where the solution of Problem 2.2 is unique. In particular, denote by $\mathbf{u}^{(1)}$ the solution associated to the data $p_i^{(1)}$ $(i = 1, \ldots, \overline{n})$ and, correspondingly, by $\mathbf{u}^{(2)}$ the solution associated to $p_i^{(2)}$ $(i = 1, \ldots, \overline{n})$. Set:

$$
\mathbf{w} = \mathbf{u}^{(1)} - \mathbf{u}^{(2)}, \qquad \delta\tilde{p} = \max_i |p_i^{(1)} - p_i^{(2)}|.
$$

By subtraction and some classical estimates (see [10]), we have :

$$
\begin{aligned}
&\frac{1}{2}\frac{d}{dt}\|\mathbf{w}\|^2 + \nu\|\nabla \mathbf{w}\|^2 + \Sigma_i R_i \int_{\Gamma_i} |\mathbf{w} \cdot \mathbf{n}|^2 d\boldsymbol{\gamma} \\
&\quad = -b(\mathbf{u}^{(2)}, \mathbf{w}, \mathbf{w}) - b(\mathbf{w}, \mathbf{u}^{(2)}, \mathbf{w}) - b(\mathbf{w}, \mathbf{w}, \mathbf{w}) + \int_{\Gamma_i} (p_i^{(1)} - p_i^{(2)}) \mathbf{w} \cdot \mathbf{n} d\boldsymbol{\gamma} \\
&\qquad \leq \frac{\nu}{2}\|\nabla \mathbf{w}\|^2 + \frac{c_6}{\nu} \sup |\mathbf{u}^{(2)}|^2 \|\mathbf{w}\|^2 + \frac{c_7}{\nu^3}\|\nabla \mathbf{u}^{(2)}\|^4 \|\mathbf{w}\|^2 + c_8 \|\mathbf{w}\| \|\nabla \mathbf{w}\|^2 + c_9 \delta\tilde{p}^2.
\end{aligned} \tag{2.19}
$$

Hence:

$$\begin{aligned}\frac{1}{2}\frac{d}{dt}\|\mathbf{w}\|^2 + (\nu - c_{10}\|\mathbf{w}\|)\|\nabla\mathbf{w}\|^2 \\ \leq c_{11}(\frac{1}{\nu}\sup|\mathbf{u}^{(2)}|^2 + \frac{1}{\nu^3}\|\nabla\mathbf{u}^{(2)}\|^4)\|\mathbf{w}\|^2 + c_9\delta\tilde{p}^2,\end{aligned} \tag{2.20}$$

Since $\mathbf{w}(0,\mathbf{x}) = \mathbf{0}$, from this inequality we deduce that there exists $T > 0$ such that:

$$\|\mathbf{w}\| \leq c \max_{0<t\leq T} \delta\tilde{p}. \tag{2.21}$$

Finally, the uniqueness of the solution can be proven by contradiction. Assume that there exist two solutions associated to the same data set. We can repeat steps (2.19), (2.20) with $\delta\tilde{p} = 0$. Then (2.21) implies that the solution is unique, and this concludes our proof.

□

REMARK 2.1. *Since* $\mathbf{w}$ *is a solenoidal function, we have the trace inequality[10] (see also (2.11)):*

$$|\int_{\Gamma_i} \mathbf{w}\cdot\mathbf{n}d\boldsymbol{\gamma}| \leq c_{12}\|\mathbf{w}\|$$

Together with (2.21), it implies in particular that the flow rates on the boundaries Γ_i *are continuous functions of the pressure data.*

3. Lumped parameters models. Modeling the whole circulatory system in terms of the Navier-Stokes equations as done in the previous Section is not affordable in practice due to its prohibitive computational cost. In this context, simplified models are often applied. They are less accurate as they cannot catch local details, however they can correctly account for systemic phenomena (like pressure pulse propagation or flow rate distribution at different environments), and have the fascination of being computationally very cheap.

The earliest and most simple global models considered in the literature are based on a representation of the circulatory system as a network of "compartments". The mathematical description of the problem moves from an analogy with electric circuits. Actually, in the Sixties electric circuits were physically built as "circulation analog simulators" (see [23]). On the ground of this analogy, a systemic representation of the circulation is given by a set of ordinary differential equations. In the multiscale perspective of the present work, such equations need to be numerically linked to the Navier-Stokes model set on a specific local region (see e.g. [16]).

In the following subsection we firstly introduce the lumped parameter model of a very simple compartment given by a compliant cylindrical pipe. This will help to clarify the physical meaning of the lumped parameters we are dealing with. Then, we will give a short outline of the lumped description of districts of specific interest (such as the heart, the heart valves, etc.), that are assembled in a network of compartments. Finally, we will discuss the most relevant mathematical features of the associated system of ordinary differential equations in view of the subsequent analysis of the multiscale model.

3.1. Lumped models for a cylindrical vessel. Let us consider a cylindrical compliant pipe of length l and radius R_0. Denote by p_{up} and p_{dw} the mean pressure

on the upstream and downstream sections, respectively. Moreover, we set

$$F_{up}(t) = \int_{\Gamma_{up}} \mathbf{u} \cdot \mathbf{n} d\boldsymbol{\gamma}, \qquad F_{dw}(t) = \int_{\Gamma_{dw}} \mathbf{u} \cdot \mathbf{n} d\boldsymbol{\gamma}$$

the upstream and downstream flow rates, respectively. We denote by $F(t)$ the flow rate at the mid-point of the pipe (Figure 3.1 left).

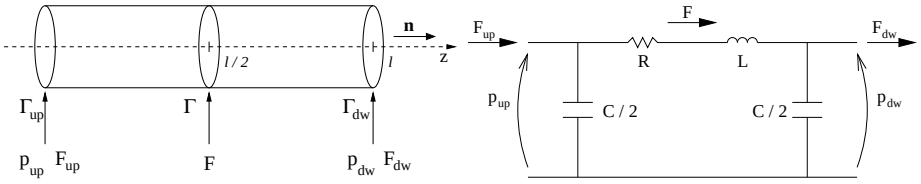

FIG. 3.1. *Location of the variables of interest upstream, downstream and the middle of a cylindrical vessel featuring finite length l (left). A lumped π-network is shown; it is equivalent to a compliant pipe with both the flow rates prescribed on the artificial sections (right).*

Suppose that $F_{up}(t)$ and $F_{dw}(t)$ are prescribed. Under suitable simplifying assumptions the momentum and mass conservation principles yield the following system of ordinary differential equations (see e.g. [16])

$$\frac{d\mathbf{y}}{dt} = A\mathbf{y} + \mathbf{b}(F_{up}, F_{dw}) \qquad t > 0 \tag{3.1}$$

where $\mathbf{y} = (p_{up}, p_{dw}, F)^T$ is the "state vector" (which depends on t),

$$A = \begin{pmatrix} 0 & 0 & -2/C \\ 0 & 0 & 2/C \\ 1/L & -1/L & -R/L \end{pmatrix}, \qquad \mathbf{b}(F_{up}, F_{dw}) = \begin{pmatrix} 2F_{up}/C \\ -2F_{dw}/C \\ 0 \end{pmatrix}.$$

The parameters R, L and C depend on the physical and geometrical properties of the pipe at hand. More precisely (see e.g. [23]):

$$R = \frac{8\nu l}{\pi R_0^4}, \; L = \frac{\rho l}{\pi R_0^2}, \; C = \frac{3\pi R_0^3 l}{2Eh} \tag{3.2}$$

where σ, E and h are the Poisson ratio, the Young modulus and the wall thickness. Equations (3.1) can be equivalently regarded as the mathematical description of an electric circuit, which is known as π-network (see Figure 3.1 right).
Note that, in the hydraulic/electric analogy, pressure and flow rate correspond to the electric voltage and current, respectively; moreover, the resistor R is related to blood viscosity, the inductor L to the inertia of blood and the capacitor C to the wall compliance. More details can be found in [16, 23].

3.2. Network models for the circulatory system. A network model of the circulatory system can be regarded as the assembly of many elementary bricks such as the one in Figure 3.1, right. However, a specific description is required for the heart action of providing the energy necessary to blood for circulation in the whole system. Heart can be considered as a couple of pumps. In particular, in [20], each ventricle

can be represented as a compliant vessel whose compliance $C(t)$ changes in time. Moreover, in order to describe the heart action, in the electric/hydraulic analogy every valve behaviour is suitably modelled by a *diode* for the current according to the value of the applied voltage drop. Precisely, one ventricle is represented by a simple brick as in Figure 3.2, where two diodes S_1 and S_2 and a compliance $C(t)$ are represented (see also [15]).

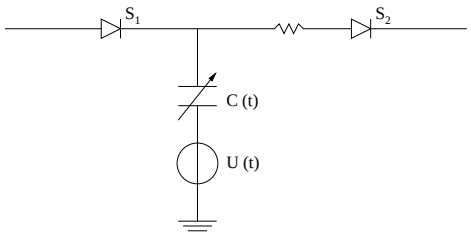

FIG. 3.2. *Scheme of a ventricle, represented by a pressure source $U(t)$ and a compliance $C(t)$ changing in time. The two valves are modelled by two diodes S_1 and S_2.*

Altogether, the whole circulation can therefore be described by differential system whose abstract form reads

$$\begin{cases} \dfrac{d\mathbf{y}}{dt} = A(\mathbf{y},t)\mathbf{y} + \mathbf{r}(\mathbf{y},t) \qquad t > 0 \\ \mathbf{y}(0) = \mathbf{y}_0 \end{cases} \tag{3.3}$$

where $\mathbf{y} \in \mathbb{R}^m$ is the vector of state variables, $A(\mathbf{y},t) \in \mathbb{R}^{m\times m}$ and $\mathbf{r}(\mathbf{y},t) \in \mathbb{R}^m$ are a matrix and a vector whose dependence on $\mathbf{y}$ is due to the presence of diodes, while the dependence on time has to be attributed to the heart ventricles compliances.

Specific instances of systems like the one in (3.3) can be found e.g. in [11, 14]. In the quoted references, lumped parameters systems featuring respectively 16 and 48 state variables for the description of the whole circulation have been proposed for a specific investigation of the coronary bed.

4. The geometrical multiscale model. We wish now to represent the whole system by an electric circuit except on a specific region Ω, where blood flow is modelled by the Navier-Stokes equations.

For the sake of simplicity, the compliance of the vessel wall is neglected, hence Ω is constant in time. The mean pressure and the flow rate through each artificial section Γ_i of Ω ($i = 1,\dots,\overline{n}$) are denoted by p_i and F_i. We will set $\mathbf{F} = (F_i)_{i=1,\dots,\overline{n}}$, where $F_i(t) = \int_{\Gamma_i} \mathbf{u}\cdot\mathbf{n}d\gamma$.

Let us assume that the network faces the district Ω by capacitors C_i and resistors R_i ($i = 1,\dots,\overline{n}$) as shown in Figure 4.1. In particular, we have put in evidence the representation in terms of a network of the vascular regions in the immediate neighborhood of the 3D model. We denote these parts of the lumped network the *bridging regions*. In this picture, we have three bridging regions corresponding to the three sections of Ω. The Navier-Stokes equations and the lumped network are actually coupled by means of interface conditions involving the flow rates and the mean pressure values in the bridging regions. More precisely, denote again by $\mathbf{y} \in \mathbb{R}^m$ the state vector of the circuit at hand. For the sake of notation, we will suppose that

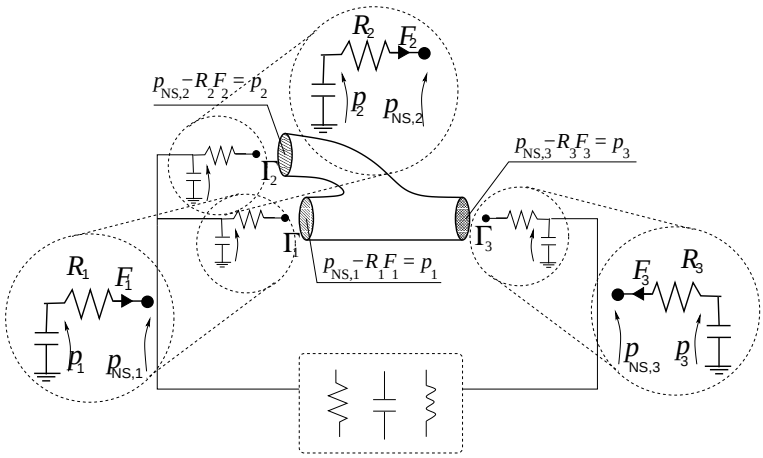

FIG. 4.1. *Scheme of coupling between the whole system and a local district. The lumped representation of the three bridging regions at the interfaces with the Navier-Stokes model is highlighted in the dashed circles. This representation is related to the interface conditions (4.3).*

the first $\overline{n}$ state variables y_i $(i = 1, \dots, \overline{n}, \overline{n} < m)$ correspond to the interface pressures $p_i(t)$. Due to the specific lumped representation of the bridging regions, the mean pressures on the Navier-Stokes interfaces are given by $p_i(t) - R_i F_i(t)$ $(i = 1, \dots, \overline{n})$. Moreover, observe that the fluxes $F_i(t)$ are not state variables of the lumped system, as no time derivatives of $F_i(t)$ occur in the mathematical description of the network.

We will assume that the network is modelled by the differential system (3.3). In particular we set

$$\mathbf{r}(\mathbf{y}, t) = \mathbf{r}_H(\mathbf{y}, t) + \mathbf{b}(\mathbf{F}(t)),$$

where, $\mathbf{r}_H$ accounts for the heart action, $\mathbf{b}$ involves the variables at the external terminals in such a way that

$$\begin{cases} b_i = \mathcal{C}_i F_i & \text{for } i = 1, \dots, \overline{n} \\ b_k = 0 & \text{otherwise} \end{cases} \tag{4.1}$$

and $\mathcal{C}_i$ are suitable constants depending on the capacitors at the interfaces.

The coupled problem reads therefore:

PROBLEM 4.1. *Given* $\mathbf{u_0} \in \mathbf{V}^*$ *and* $\mathbf{y}_0 \in \mathbb{R}^m$, *find* $\mathbf{u} \in L^2(0, T; \mathbf{V})$ *and* $\mathbf{y} \in \mathbf{L}^\infty(0, T)$ *such that for every* t

$$\begin{cases} \dfrac{d\mathbf{y}}{dt} = A(\mathbf{y}, t)\mathbf{y} + \mathbf{r}_H(\mathbf{y}, t) + \mathbf{b}(\mathbf{F}(t)) \\ \left(\dfrac{\partial \mathbf{u}}{\partial t}, \boldsymbol{\varphi}\right) + a(\mathbf{u}, \boldsymbol{\varphi}) + b(\mathbf{u}, \mathbf{u}, \boldsymbol{\varphi}) = c(\boldsymbol{\varphi}) \qquad \forall \boldsymbol{\varphi} \in \mathbf{V}^* \end{cases} \tag{4.2}$$

with $\mathbf{y}(0) = \mathbf{y}_0$, $\mathbf{u}|_{t=0} = \mathbf{u}_0$, *where, as stated above, the first* $\overline{n}$ *entries of the state vector* $\mathbf{y}$ *correspond to the interface pressures, in such a way that the mean pressures at the interface boundaries* Γ_i *are given by:*

$$p_{\Gamma_i}(t) = p_i(t) - R_i F_i(t) = y_i(t) - R_i F_i(t) \quad i = 1, \dots, \overline{n} \tag{4.3}$$

and, by definition, the entries of the vector $\mathbf{F}$ *are given by:*

$$F_i(t) = \int_{\Gamma_i} \mathbf{u} \cdot \mathbf{n} d\gamma \quad i = 1, \ldots, \overline{n}. \tag{4.4}$$

In (4.2), the bilinear form $a(\cdot,\cdot)$, the trilinear form $b(\cdot,\cdot,\cdot)$, as well as the functional $c(\cdot)$ are the same introduced in (2.5a), (2.5b), (2.5c), (2.5d). Observe that $c(\cdot)$ in (4.2) is a function of the vector $\mathbf{y}$, and, in particular, of its first $\overline{n}$ components.

In Problem 4.1 we match a local 3D model, for a domain of the order of a few centimeters, with a systemic model, covering a much wider region. The level of detail provided by the two models is obviously not the same. This difference is evident and relevant at the interfaces. On one hand, the ODE model considers mean data, namely $p_i(t)$ and $F_i(t)$, as specified in (4.3) and (4.4). On the other hand, the Navier-Stokes model would require pointwise conditions like (2.4). In Problem 4.1, this difference is in fact faced by a natural treatment of the boundary conditions, as suggested, in a similar context, in [10]. In particular, the variational formulation for the Navier-Stokes problem considered in (4.2) accounts for the interface data (4.3) in a natural way, which corresponds to force a pointwise relation like (2.4). Besides, (4.4) states the relation between the mean data of velocity considered by the systemic side and the pointwise velocity field of the Navier-Stokes equations. In the next Section, we will see that this strategy ensures the well posedness of the coupled problem. In §5.3, however, we will return on this issue and in particular on the impact of substituting (4.3) with (2.4).

5. Well posedness analysis of the multiscale model. In this Section, we prove a local-in-time existence result for Problem 4.1, by reformulating it as a fixed point problem. We will prove that the fixed point map $\mathcal{T}$ is a *compact operator* mapping a bounded subset of a Banach space into itself, to which the classical Schauder theorem can be applied.

It is worthwhile to observe that a similar fixed-point approach we have adopted in [16] for the numerical solution of this multiscale problem.

5.1. An auxiliary linear lumped model. In order to define the operator $\mathcal{T}$, we introduce the following ordinary differential system, which is a linear counterpart of (3.3):

$$\begin{cases} \dfrac{d\mathbf{y}}{dt} = A(\mathbf{z},t)\mathbf{y} + \mathbf{r}_H(\mathbf{z},t) + \mathbf{b}(\mathbf{F}(t)) & t > 0 \\ \mathbf{y}(0) = \mathbf{y}_0 \end{cases} \tag{5.1}$$

where the vector of fluxes $\mathbf{F}(t)$, matrix $A(\mathbf{z},t)$ and vectors $\mathbf{r}_H(\mathbf{z},t)$ and $\mathbf{b}(\mathbf{F}(t))$ are defined as in (3.3) and $\mathbf{z} \in \mathbf{L}^\infty(0,T)$ is a given vector function.

Suppose that there exist two constants $C_A, C_H > 0$ such that

$$\|A(\mathbf{z},t)\|_2 \le C_A \quad \text{and} \quad |\mathbf{r}_H(\mathbf{z},t)| \le C_H \qquad \forall \mathbf{z} \in \mathbf{L}^\infty(0,T), \forall t \in (0,T). \tag{5.2}$$

Finally, define $c_0 = \max_i(\mathcal{C}_i^2)$, where $\mathcal{C}_i$ are given in (4.1), so that

$$|\mathbf{b}(\mathbf{F}(t))|^2 \le c_0 \sum_{i=1}^{\overline{n}} |F_i(t)|^2 \quad \forall t > 0. \tag{5.3}$$

Classical results (see e.g. [19]) yield the existence and uniqueness of the solution of the linear system (5.1). Moreover, using the Gronwall Lemma, we obtain:

$$(5.4)\quad |\mathbf{y}(t)|^2 \leq \left(|\mathbf{y}_0|^2 + C_H^2 t + c_0 \sum_{i=1}^{\overline{n}} \int_0^t |F_i(s)|^2 \, ds \right) \exp(2(1+C_A)t), \qquad \forall t > 0.$$

5.2. The main result. For any $\sigma > 0$ we consider the subset of $\mathbf{L}^\infty(0,T)$:

$$(5.5)\quad \mathcal{B}_{\sigma,T} = \{\mathbf{z} \in \mathbf{L}^\infty(0,T) : |\mathbf{z}| \leq \sigma\}.$$

Consider Problem 2.1 and a vector $\mathbf{z} \in \mathcal{B}_{\sigma,T}$. Denote by $\mathcal{L}_{NS}$ the operator mapping $\mathbf{z}(t)$ into the solution $\mathbf{u}(\mathbf{x},t)$ of Problem 2.1:

$$\mathbf{u} = \mathcal{L}_{NS}\mathbf{z}.$$

More precisely, we solve Problem 2.1 with the pressure data provided by the first $\overline{n}$ components of $\mathbf{z}$. Then, we set $\mathbf{F}(t)$ the vector whose entries $F_i(t)$ are function of $\mathbf{u}(\mathbf{x},t)$ according to (4.4) and solve the linear ordinary differential system (5.1). In this way, we implicitly define the operator $\mathcal{L}_{NET}$, mapping $\mathbf{u}(\mathbf{x},t)$ into $\mathbf{y}(t)$,

$$\mathbf{y} = \mathcal{L}_{NET}\mathbf{u}$$

and therefore a composite operator:

$$\mathcal{T} = \mathcal{L}_{NET} \cdot \mathcal{L}_{NS} : \mathcal{B}_{\sigma,T} \to \mathbf{L}^\infty(0,T), \quad \mathbf{z} \to \mathbf{y} = \mathcal{T}\mathbf{z}.$$

At this stage, we can easily see that if $\mathbf{y}$ is a fixed point of $\mathcal{T}$, i.e. $\mathbf{y} = \mathcal{T}\mathbf{y}$, then, the couple $(\mathbf{y}, \mathbf{u} = \mathcal{L}_{NS}\mathbf{y})$ is a solution of Problem 4.1. We are therfore left to prove that $\mathcal{T}$ has a fixed point.

PROPOSITION 5.1. *Suppose that the initial data* $\mathbf{y}_0$ *and* $\nabla\mathbf{u}_0$ *are small enough, and, in particular, that:*

$$(5.6)\quad |\mathbf{y}_0| < \sigma \qquad \|\nabla\mathbf{u}_0\| \leq \sigma_1.$$

where σ *and* σ_1 *are chosen in such a way that Problem 2.2 is well posed as stated in Proposition 2.1. Moreover, suppose that (5.2) and (2.14) hold. Consequently, there exists* $\tilde{T}$ $(0 < \tilde{T} \leq T)$ *such that* $\mathcal{T}$ *is a compact operator mapping* $\mathcal{B}_{\sigma,\tilde{T}}$ *into itself. Then,* $\mathcal{T}$ *admits at least one fixed point in* $\mathcal{B}_{\sigma,\tilde{T}}$.

Proof. Let $\mathbf{z}$ be a vector in $\mathcal{B}_{\sigma,T}$, and define $\mathbf{y} = \mathcal{T}\mathbf{z}$. Note that from (5.4) $\mathbf{y} \in \mathbf{L}^\infty(0,T)$. Let us prove that there exists a time interval $\mathcal{I} \equiv (0,\widetilde{T})$ such that $\mathbf{y} \in \mathcal{B}_{\sigma,\tilde{T}}$ for $t \in \mathcal{I}$. In fact, this proves that $\mathcal{T}$ maps $\mathcal{B}_{\sigma,\tilde{T}}$ into itself. According to the notation of §2, set $\tilde{p} = \sup_{t\geq 0} \sum_{i=1}^{\overline{n}} |p_i(t)|$ where as usual p_i are the first $\overline{n}$ entries of $\mathbf{z}$. Since $\sum_{i=1}^{\overline{n}} |p_i(t)|^2 \leq |\mathbf{z}(t)|^2$ for every t, it follows that $\tilde{p} \leq \sigma$. Then, according to Proposition 2.1, there exists a unique solution $\mathbf{u}$ of Problem 2.2 in a time interval $(0,T)$ such that

$$(5.7)\quad \|\nabla\mathbf{u}(t)\| \leq \sigma_1 \quad \forall t \in (0,T).$$

Furthermore, consider the system (3.3) with $F_i(t)$ as in (4.4). If $\boldsymbol{\varphi}$ is any function of $\mathbf{V}^*$ and Γ any subset of $\partial\Omega$, the inequality

$$(5.8)\quad \left| \int_\Gamma \boldsymbol{\varphi} \cdot \mathbf{n} d\gamma \right| \leq c_5 \|\nabla\boldsymbol{\varphi}\|$$

holds for a constant c_5 whose value depends on the Poincaré inequality. Then, owing to (5.7) and (5.8), $\mathbf{b}(\mathbf{F}(t))$ in (5.3) belongs to $\mathbf{L}^2(0,T)$, whence the Cauchy problem (5.1) is well posed in $(0,T)$. Denote by $\mathbf{y}$ its unique solution. In particular, since $|F_i(t)| \leq c_5 \|\nabla \mathbf{u}(t)\|$, from (5.4) it follows that

$$|\mathbf{y}(t)|^2 \leq \left(|\mathbf{y}_0|^2 + C_H^2 t + \overline{n} c_0 c_5^2 \int_0^t \|\nabla \mathbf{u}(s)\|^2 ds \right) \exp((2 + C_A)t). \tag{5.9}$$

Under assumption (5.6) it is possible to verify that there exists a positive $\tilde{T}$ such that the following inequality

$$|\mathbf{y}_0|^2 + C_H^2 t + \overline{n} c_0 c_5^2 \int_0^t \|\nabla \mathbf{u}(s)\|^2 ds \leq \sigma^2 \exp(-(2 + C_A)t) \tag{5.10}$$

holds for all $0 \leq t \leq \tilde{T}$. Indeed $\tilde{T}$ corresponds to the intersection point between the monotonically increasing curve $|\mathbf{y}_0|^2 + C_H^2 t + \overline{n} c_0 c_5^2 \int_0^t \|\nabla \mathbf{u}(s)\|^2 ds$, and the monotonically decreasing one $\sigma^2 \exp(-(2 + C_A)t)$ (see Figure 5.1). Thus, thanks to (5.9) we

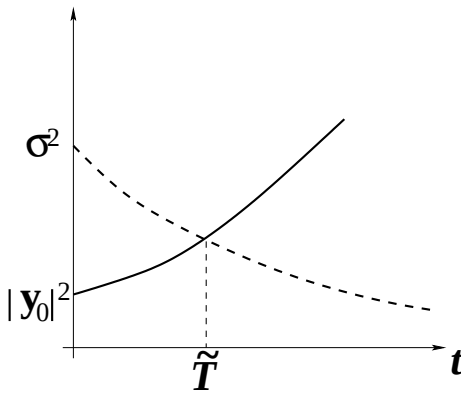

FIG. 5.1. *Intersection between the curves* $|\mathbf{y}_0|^2 + C_H^2 t + \overline{n} c_0 c_5^2 \int_0^t \|\nabla \mathbf{u}(s)\|^2 ds$ *(solid line) and* $\sigma^2 \exp(-(2 + C_A)t)$ *(dash-dotted line).*

have

$$|\mathbf{y}(t)| \leq \sigma \tag{5.11}$$

for each $t \in (0, \tilde{T})$. Therefore, in $(0, \tilde{T})$ $\mathcal{T}$ maps $\mathcal{B}_{\sigma,\tilde{T}}$ into itself.

Moreover, $\mathcal{T} = \mathcal{L}_{NET} \cdot \mathcal{L}_{NS}$ is continuous. Indeed, this follows from the continuity of the two maps $\mathcal{L}_{NS}$ and $\mathcal{L}_{NET}$; $\mathcal{L}_{NS}$ is continuous as proven in (2.21), while the continuity of $\mathcal{L}_{NET}$ is an immediate consequence of the continuity of $\mathbf{b}(\cdot)$ defined in (4.1) and the fact that the ordinary differential system at hand (5.1) is linear.

Having proven the continuity of $\mathcal{T}$, we now need to prove its compactness. Since the set $\mathcal{B}_{\sigma,\tilde{T}}$ is bounded by construction, we need simply to prove the compactness of the range of $\mathcal{B}_{\sigma,\tilde{T}}$ according to $\mathcal{T}$. We have already verified that this set is bounded. Moreover, from (5.1) we have for all $t \in \mathcal{I}$:

$$\left| \frac{\partial \mathbf{y}}{\partial t} \right| = |A(\mathbf{z},t)\mathbf{y} + r_H(\mathbf{z},t) + \mathbf{b}(\mathbf{F})| \leq C_A \sigma + C_H + C\sigma_1 = M$$

where the constant M does not depend on t. We can therefore conclude that the image of a bounded set in $\mathbf{L}^\infty(0,\tilde{T})$ according to the map $\mathcal{T}$ is bounded and equicontinuous. Thanks to the Ascoli-Arzelà Theorem,[26] this means that the image of a bounded set according to $\mathcal{T}$ is compact. Since $\mathcal{T}$ is continuous, we conclude that $\mathcal{T}$ is *compact*.

The (local-in-time) existence of the solution of the multiscale Problem 4.1 follows from the Schauder fixed point principle ([26]).

□

It is worthwhile to point out that, if $(\mathbf{u},\mathbf{y})$ satisfies Problem 4.1, then there exists a unique function $p \in L^2(0,\tilde{T};L^2(\Omega))$ such that the couple $(\mathbf{u},p)$ is solution of the Navier-Stokes submodel. Indeed, the map $\mathcal{L}_p : \mathbf{V} \to \mathbb{R}$ such that $\mathcal{L}_p(\boldsymbol{\varphi}) = \frac{d}{dt}(\mathbf{u},\boldsymbol{\varphi}) + a(\mathbf{u},\boldsymbol{\varphi}) + b(\mathbf{u},\mathbf{u},\boldsymbol{\varphi})$ belongs to $\mathbf{V}'$ and vanishes on $\mathbf{V}^*$. Therefore, by well known results (see e.g.[8]) there exists a function $p \in L^2(\Omega)$ (which is unique up to an additive constant), such that $\mathcal{L}_p(\boldsymbol{\varphi}) = (p,\nabla\boldsymbol{\varphi})$ for all $\boldsymbol{\varphi} \in \mathbf{V}$. Thanks to conditions (2.4), p is the unique function such that $(\mathbf{u},p)$ solves the Navier-Stokes problem.

REMARK 5.1. *The initial bounds assumed by hypothesis in (5.6) actually hold in $\mathcal{I}$, in the sense that:*

$$|\mathbf{y}(t)| \le \sigma \qquad \textit{and} \qquad \|\nabla\mathbf{u}(t)\| \le \sigma_1 \tag{5.12}$$

for each $t \in (0,\tilde{T})$. This is an immediate consequence of the estimates found in proving Propositions 2.1 and 5.1.

REMARK 5.2. *In §3 we have pointed out that systemic models can be obtained by considering the circulation as a set of regions connected one to the others. Starting from a 3D description of blood flow in each region (based on the Navier-Stokes equations), we obtain a simplified mathematical description carrying out a space average of the basic equations of mass and momentum conservation. The actual values of the parameters depend on the geometrical and physical features of the compartment at hand (see (3.2)). As an example, in the case of a compliant straight pipe, the value of the resistance parameter R is a function of the blood viscosity ν, the radius of the pipe R_0 and the length of the compartment l.*

In the multiscale model, interface conditions (4.3) involve the parameters of the lumped network. In particular, conditions (4.3) depend on the resistence parameters R_i featuring the bridging regions interposed between the local model and the remainder of the circulation. In this context, assumption (2.14) can be regarded as a constraint on geometry of the bridging regions. In particular, suppose that these regions are cylindrical vessels. Owing to (3.2), (2.14) reads $16lc_2c_4 < \pi R_0^4$. In fact, the assumption (2.14) can be reinterpreted as a constraint on the length l of the bridging region which must be sufficiently small. In other words, a suitable lumped representation, where the bridging districts have been suitably chosen, can always satisfy (2.14).

5.3. Different splittings of the coupled problem. In the proof of Proposition 5.1 we have analysed the coupled problem by means of a splitting of the multiscale problem into a local Navier-Stokes problem and a global ordinary differential system. In this context, at the first step of the splitting, the interface conditions (4.3) have played the role of boundary conditions for the Navier-Stokes problem. On the other hand, the interface conditions (4.4) has been accounted for in the second step through the forcing terms of the lumped parameters system.

As pointed out in §4, there is a difference between the data accounted for at the interfaces of the two models. In the perspective of the splitting, we are now in position of specifying how this difference is faced. Indeed, (4.3) is not enough as boundary

condition for a 3D Navier-Stokes problem, since it prescribes average data on the interfaces, while three conditions would be required pointwise ([21]). However, the selected variational formulation introduced in Problem 2.1 and 4.1 corresponds to the natural treatment of *defective* conditions firstly introduced for the mean pressure drop problem in [10].

More precisely, the weak formulation (4.2) embodies condition (2.4) as natural condition. In the special case of a cylindrical domain with boundary sections orthogonal to the vessel axis, condition (2.4) does actually reduce to (4.3), as the viscous forces $\nu\nabla\mathbf{u}\cdot\mathbf{n}$ vanish on Γ_i. Although the latter circumstance does not occur in domains of general shape, nonetheless the extra-conditions stemming from (2.4) with respect to (4.3) are satisfied in a weak sense and therefore yield mild perturbation on the associate solution.

The role of the interface conditions in the splitting procedure is in fact naturally driven by the specific topology of the network at the interfaces. In our case, the interface flow rates are not state variables of the lumped system, and, therefore, they are well suited to play the role of a forcing term for the ordinary differential system. However, depending on the choice of the bridging regions, the matching between the network and the Navier Stokes system could be pursued, for instance, by interchanging the role of flux and pressure at the interfaces. When splitting the coupled problem,

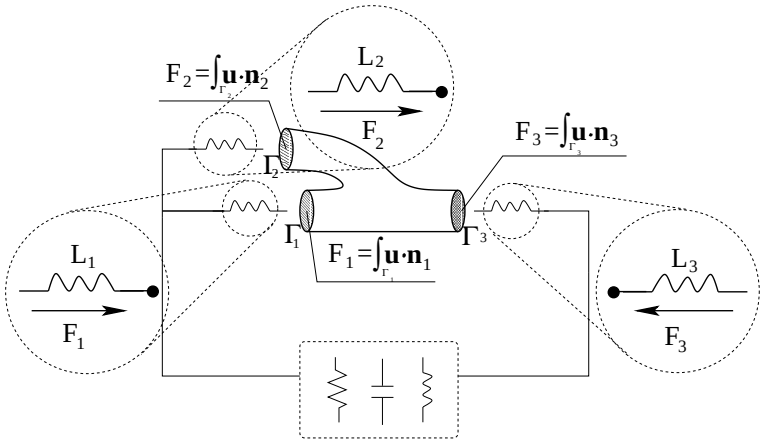

FIG. 5.2. *Scheme of coupling between the whole system and a local district where the bridging regions are given by inductors.*

we should suppose that the flow rates are provided to the Navier-Stokes system by the network, which in turn receives pressure data. For instance, in the network configuration of Fig. 5.2, the interface pressure is not a state variable of the lumped system, so it is a good candidate for being a forcing term of the ordinary differential system, provided by the Navier-Stokes solution. On the other hand, the interface flow rates, which in the electric analogy correspond to the current at the interfaces and are state variables for the system, become boundary data for the Navier-Stokes problem. In a way similar to the (generalized) mean pressure problem (conditions (4.3)), the prescription of boundary fluxes is not enough to make the Navier-Stokes problem well posed. The defective data still need to be suitably completed. A theoretical analysis of this problem has been carried out in [10], while a reformulation of this

problem that is more suitable for the numerical approximations is provided in [6]. In the perspective of the present work, the results in Proposition 5.1 can be extended to this case as well. Actually, a fixed point approach can be adopted in the proof, in a completely similar way to the one adopted here, starting from the well-posedness analysis of the individual submodels.

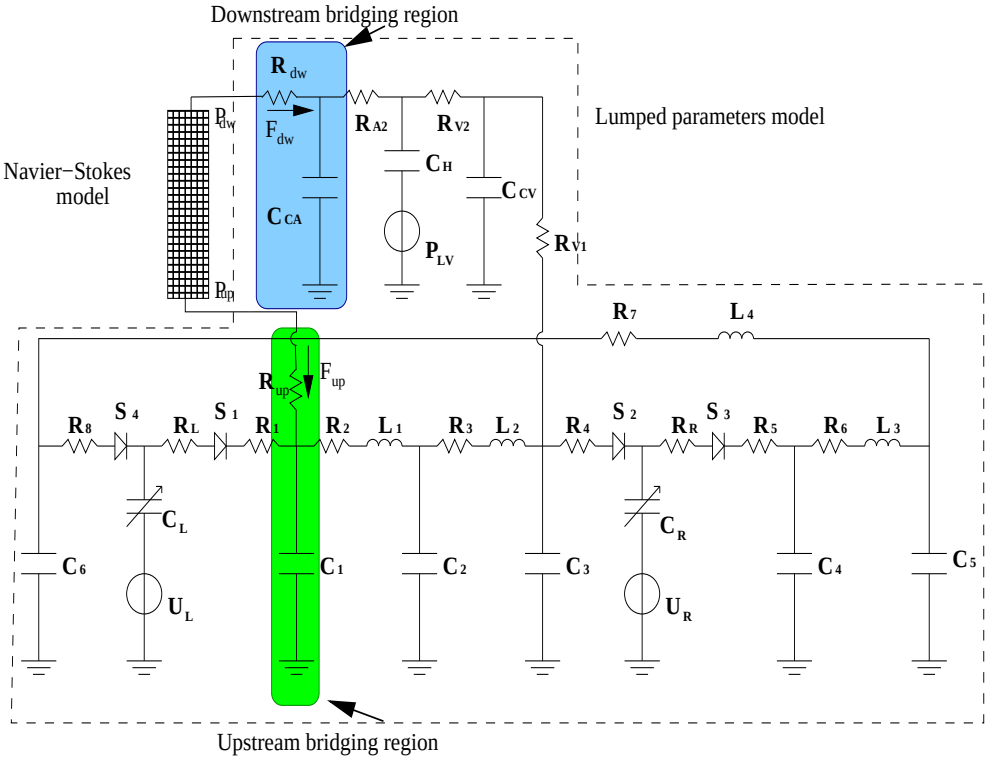

FIG. 5.3. *Representation of the multiscale test case.*

6. A numerical test case. In this Section, we illustrate some numerical results on a test case based on the Womersley solution for the Navier-Stokes equations (see [24]).

Consider a flow between two infinite planes where a periodic-in-time pressure gradient is prescribed. Let the two planes be at distance d in the frame of reference (x_1, x_2). In particular, if the pressure gradient is given by:

$$\nabla p = A \sin(\omega t),$$

the flow field can be analytically determined, providing in 2D the analog of the Womersley solution, that has been obtained for a 3D cylindrical domain (see [24, 17]). In particular, the transversal velocity u_2 is null, while the axial velocity u_1 is:

$$u_1 = \sum_{k=0}^{\infty} \gamma_{2k+1} \sin\left(\frac{(2k+1)\pi}{d} x_2\right) \tag{6.1}$$

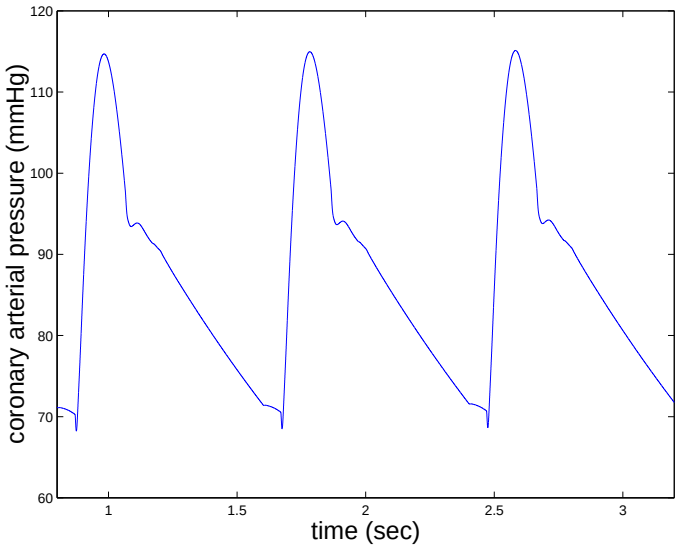

FIG. 5.4. *Pressure drop of the multiscale simulation applied to the 2D region.*

where, setting $\beta = \dfrac{\nu\pi^2}{d^2}$,

$$\gamma_i = \frac{4A}{\pi i(i^4\beta^2+\omega^2)}\left(i^2\beta\sin(\omega t)+\omega e^{-i^2\beta t}-\omega\cos(\omega t)\right)$$

Observe that (like for the Poiseuille flow) the non-linear term in the Navier-Stokes equations vanishes, independently of A and ω, since, due to the particular morphology and the boundary data independent of x_2, the velocity field is orthogonal to its gradient. Therefore, for more complex periodic pressure differences, the analytical solution can be determined by expanding the pressure drop in a Fourier series, and superimposing the contribution of each term accordingly.

The variational strategy illustrated above has been succesfully adopted in [22] for computing the Womersley solution (6.1) on a couple of finite length of planes, that means a 2D rectangular pipe, featuring an upstream and a downstream section. In the multiscale perspective, we have coupled such 2D rectangular pipe with a lumped parameter model, given in Fig. 5.3. The pressure difference applied to the 2D region is periodic (see Fig. 5.4), so we can compute analytically the local flow Womersley solution. In Tab 1 we illustrate the $L^2(\Omega)$ errors at different instants of the heart beat.

These numerical results confirm the correctness of our approach and the well posedness of the multiscale model stated in the present work.

Beyond this academic test case, numerical results obtained in more realistic contexts, still based on the approach of the present work, can be found in [16] and in [2, 3, 4]. In these references the adoption of geometrical multiscale models has revealed very promising for analysing, by means of numerical simulations, the dynamics of flow patterns in morphologically complex vascular districts in the context of pediatric surgery. The goal was to identify some "optimal" design for surgical interventions. Fig. 5.5 (taken from [4], courtesy of the authors) illustrates some numerical results obtained with the geometrical multiscale approach of the present work

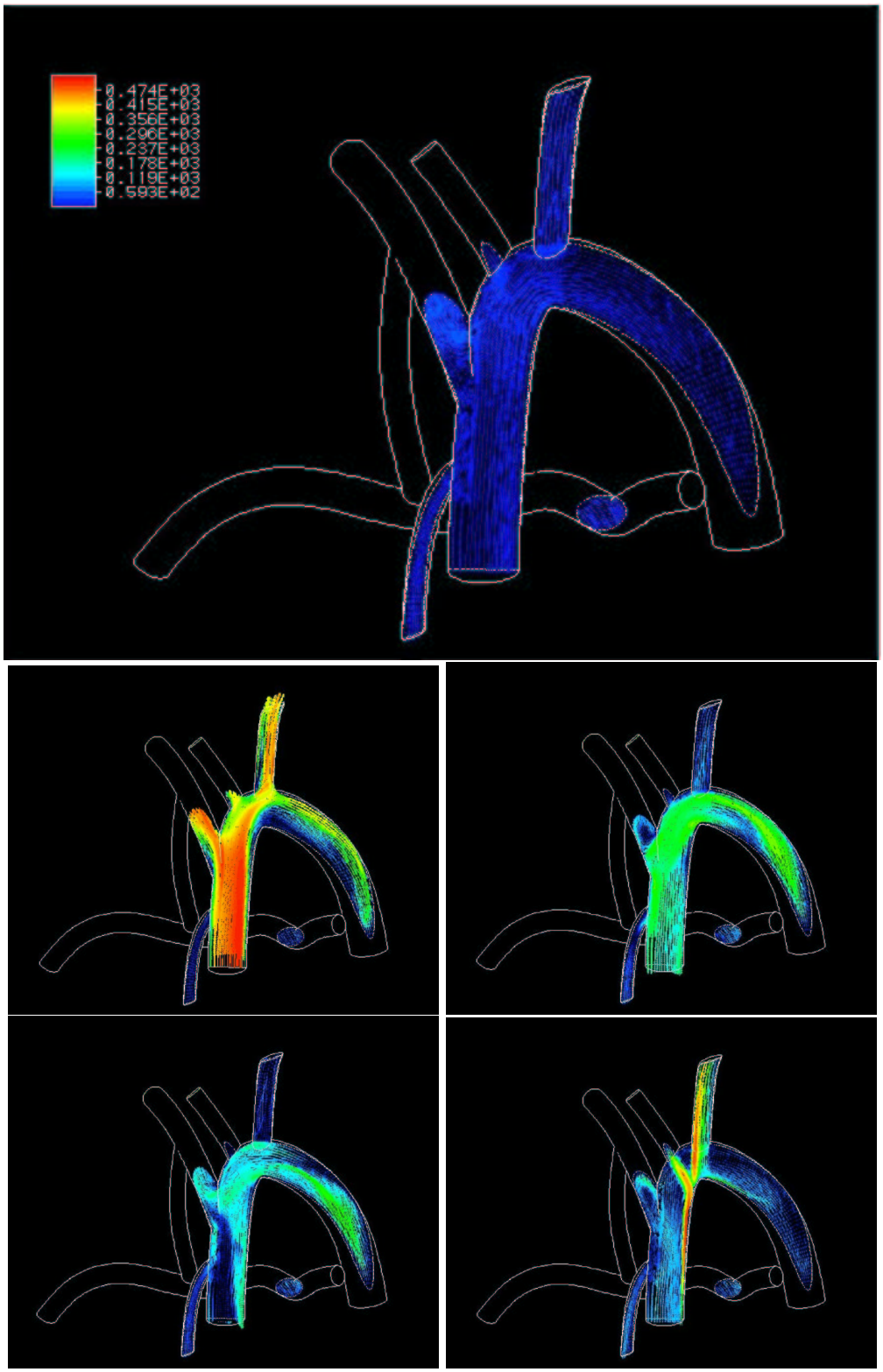

FIG. 5.5. *Simulation of a complex vascular districts (Total Cavo-Pulmonary Connections): velocity fields at different instants of the heart beat. These are the 3D results of a multiscale simulations, allowing a realistic boundary data prescription. See [4] for more details.*

TABLE 6.1
Relative errors in the Womersley test case during a heart beat. The heart beat duration is fixed to 0.8 *s.*

$\frac{t}{T_{beat}}$	$\frac{\|\mathbf{u}_{Womersley} - \mathbf{u}_{computed}\|}{\|\mathbf{u}_{Womersley}\|}$
0.125	6.0×10^{-4}
0.250	2.9×10^{-6}
0.375	2.4×10^{-5}
0.500	1.4×10^{-4}
0.625	1.1×10^{-6}
0.750	1.7×10^{-6}
0.875	1.8×10^{-6}
1.000	2.5×10^{-6}

for the ascending aorta region after a surgical intervention (the so-called TCPC, Total Cavo-Pulmonary Connection). Thanks to the multiscale approach, it has been possible to compute physiological velocity profiles and secondary flow patterns which were not captured in previous simulations, based on the prescription of incorrect (even if realistic) essential boundary velocity data.

Acknowledgements. The authors wish to thank Prof. S. Salsa for several useful suggestions, Dr. S. Ragni for having collaborated to an early version of this paper and carried out the numerical simulations of Tab. 6.1, Prof. G. Dubini and Dr. F. Migliavacca for having provided the numerical results of Fig. 5.5.

REFERENCES

[1] J. P. ARCHIE, R. P. FELDTMAN, (1981) *Critical stenosis of the internal carotid artery*, Surgery, 89 (1981), pp. 67–70.

[2] K. LAGANÀ, G. DUBINI, F. MIGLIAVACCA, R. PIETRABISSA, G. PENNATI, A. VENEZIANI, A. QUARTERONI, *Multiscale modelling as a tool to prescribe realistic boundary conditions for the study of surgical procedures*, Biorheology, to appear (2002).

[3] G. DUBINI, F. MIGLIAVACCA, R. PIETRABISSA, A. QUARTERONI, S. RAGNI, A. VENEZIANI, *From the global cardiovascular system hemodynamics down to the local blood motion: preliminary applications of a multiscale approach*, Proceedings of European Congress on Computational Methods in Applied Sciences and Engineering - ECCOMAS 2000 (2000)

[4] G. DUBINI, F. MIGLIAVACCA, *in preparation.*

[5] L. FORMAGGIA, J. F. GERBEAU, F. NOBILE, A. QUARTERONI, *On the coupling of 3D and 1D Navier-Stokes equations for flow problems in compliant vessels*, Comp. Math. Appl. Mech. Eng., 191 (2001), pp. 561–582

[6] L. FORMAGGIA, J. F. GERBEAU, F. NOBILE, A. QUARTERONI, *Numerical treatment of Defective Boundary Conditions for the Navier-Stokes equation*, SIAM J Num Anal to appear (2002)

[7] L. FORMAGGIA, F. NOBILE, A. QUARTERONI, A. VENEZIANI, *Multiscale modelling of the circulatory system: a preliminary analysis. Comp. Vis. Science*, 2 (1999), pp. 75–83.

[8] V. GIRAULT, P. RAVIART, *Finite Element Methods for Navier-Stokes Equations. Theory and Algorithms*, Springer-Verlag Series in Computational Mathematics n.5, New York (1991)

[9] J. HEYWOOD, R. RANNACHER, *Finite element approximation of the nonstationary Navier-Stokes problem. I. Regularity of solutions and second-order error estimates for spatial discretization*, SIAM J. Numer. Anal., 19 (1982), pp. 275–311.

[10] J. HEYWOOD, R. RANNACHER, S. TUREK, *Artificial boundaries and flux and pressure conditions for the Incompressible Navier-Stokes Equations*, Int. J. Num. Meth. Fl., 22 (1996), pp. 325–352.

[11] F. INZOLI, F. MIGLIAVACCA, S. MANTERO, *Pulsatile flow in an aorto-coronary bypass 3-D model*, in Biofluid Mechanics Proceedings of the 3rd International Symposium, ed. D. Liepsch, VDI Verlag, (1994).

[12] J. L. LIONS, E. MAGENES, *Problèms aux Limites non Homogènes et Applications, 1.*, Dunod, Paris (1969).

[13] A. Noordergraf, H. Boom, P. Verdouw, *A human systemic analog computer* In 1st Congr. Soc. for Ballistocardiographic Res., A. Noordergraf ed. (1960)

[14] G. Pennati, F. Migliavacca, G. Dubini, R. Pietrabissa, M. R. de Leval, *A mathematical model of circulation in the presence of the bidirectional cavopulmonary anastomosis in children with a univentricular heart*, Med. Eng. Phys., 19 (1997), pp. 223–234.

[15] F. Hoppensteadt, C. Peskin, *Mathematics in Medicine and the Life Sciences* Springer-Verlag, New York (1992)

[16] A. Quarteroni, S. Ragni, A. Veneziani, *Coupling between lumped and distributed models for blood flow problems*, Comp. Vis. Science, 4 (2001), pp. 111–124

[17] A. Quarteroni, M. Tuveri, A. Veneziani, *Computational vascular fluid dynamics: problems, models and methods*, Comp. Vis. Science, 2 (2000), pp. 163–197.

[18] V. C. Rideout, D. E. Dick, (1967) *Difference-Differential Equations for Fluid Flow in Distensible Tubes*, IEEE Transactions on Bio-Medical Engineering, Vol. BME-14, NO.3, pp. 171–177.

[19] G. Birkhoff, G.C. Rota *Ordinary Differential Equations*, J. Wiley and Sons, New York (1989)

[20] K. Sagawa, H. Suga, K. Nakayama, *Instantaneous pressure-volume ratio of the left ventricle versus instantaneous force-length relation of papillary muscle* in Cardiovascular System Dynamics, J. Baan, A. Noordergraaf, and J. Raines, eds., M.I.T. Press, Cambridge, MA (1978), pp. 99-105.

[21] R. Temam, *Navier-Stokes Equations and Nonlinear Functional Analysis*, Society for Industrial and Applied Mathematics (1984).

[22] A. Veneziani, *Boundary conditions for blood flow problems*, in Proceedings of ENUMATH 97 (Heidelberg), R. Rannacher et al. eds., World Sci. Publishing, River Edge, NJ (1998), pp. 596–605.

[23] N. Westerhof, F. Bosman, C. J. De Vries, A. Noordergraaf, *Analog studies of the human systemic arterial tree*, J. Biomech., 2 (1969), pp. 121–143.

[24] J. Womersley, *Method for the calculation of velocity, rate of flow and viscous drag in arteries when the pressure gradient is known*, J. Physiol., 127 (1955), pp. 553–563

[25] W. Xie, (1995) *Integral representations and L^∞ bounds for solutions of the Helmholtz equation on arbitrary open sets in $\mathbb{R}^2$ and $\mathbb{R}^3$*, Diff. Int. Eqn., 8 (1995) pp. 689–698.

[26] E. Zeidler, *Applied Functional Analysis*, Springer-Verlag, New York (1991)